

Utilization of APTES-functionalized coconut waste-based cellulose microfiber/zeolitic-imidazolate framework-8 composite for curcumin delivery



M.G. Wijanarko^{a, b, g}, A.J. Widagdo^{a, b, g}, M.S. Ismadji^{a, g}, K. Kusuma^{a, c, g},
M. Yuliana^{a, b, d, *}, S. Ismadji^{a, d}, S.B. Hartono^{a, d}, J. Lie^{a, b, d}, H. Shu^e, H. Abdullah^e,
G.T.M. Kadja^f, C.J. Wijaya^{a, d}, F.E. Soetaredjo^{a, d}

^a Department of Chemical Engineering, Widya Mandala Surabaya Catholic University, Kalijudan 37, Surabaya 60114, Indonesia

^b Chemical Engineering Master Program, School of Graduate Studies, Widya Mandala Surabaya Catholic University, Kalijudan 37, Surabaya 60114, Indonesia

^c Key Laboratory for Biorheological Science and Technology – Ministry of Education, State and Local Joint Engineering Laboratory for Vascular Implants, Bioengineering College, Chongqing University, Chongqing 400044, China

^d Collaborative Research Center for Zero Waste and Sustainability, Kalijudan 37, Surabaya 60114, Indonesia

^e Department of Industrial Engineering, Universitas Prima Indonesia, Medan, Indonesia

^f Department of Chemistry, Institut Teknologi Bandung, Ganesha 10, Bandung 40132, Indonesia

ARTICLE INFO

Article history:

Received 15 December 2022

Received in revised form

9 January 2023

Accepted 14 January 2023

Available online 24 January 2023

Keywords:

Coconut waste

Cellulose microfibers

Zeolitic-imidazolate framework-8

Composite material

Drug delivery system

Curcumin

ABSTRACT

With more than 7 million tons of coconut husk generated annually, this study proposes to fabricate the composite of coconut waste-based cellulose microfibers and zeolitic imidazolate framework-8 functionalized with (3-aminopropyl)-triethoxysilane (APTES-CMF/ZIF-8), which is used for curcumin uptake/release. The surface area and pore volume of APTES-CMF/ZIF-8 are found, respectively, at 247.6 m²/g and 0.21 m³/g. The morphology study also shows that the waste-based CMF possesses a uniform width at 5–10 μm, and a length of up to several tens of microns, while the impregnated ZIF-8 has a rhombic dodecahedron shape with a particle diameter of 300–400 nm. The behavior of the curcumin uptake using APTES-CMF/ZIF-8 is elucidated via kinetics, isotherm, and thermodynamic studies. The maximum curcumin adsorption reaches 626.4 mg/g at the following condition: APTES-CMF/ZIF-8 loading (m_c) = 0.1% (w/w), uptake duration (t) = 1440 min, temperature (T) = 30 °C, and initial curcumin concentration of 1000 mg/L. This uptake follows the pseudo-second-order law and monolayer mechanism, with the fast migration of curcumin from the bulk solution to the surface of APTES-CMF/ZIF-8 as the rate-governing step. The curcumin and APTES-CMF/ZIF-8 interaction is driven by the electron exchange between both molecules. The release study of curcumin from Cur@APTES-CMF/ZIF-8 complies with the slow-first-order model. Moreover, the cumulative release is monitored at 74.2% at pH 5.5 and 47.9% at pH 7.4, signifying the pH-responsiveness of APTES-CMF/ZIF-8.

© 2023 Elsevier Ltd. All rights reserved.

1. Introduction

Curcumin has recently received numerous attention due to its wide spectrum of biological and pharmacological activities [1,2]. Exhibiting high anti-inflammatory, antioxidant, anticancer, and neurotrophic activities, it is widely used to treat gallbladder

disease, cough, diabetic ulcers, liver disease, rheumatism, and sinusitis. Recent publications also indicate that curcumin can inhibit the growth of various cancer cells, including skin, gastric, duodenal, and colon cancers [3–5]. It suppresses cell proliferation and cell cycle progression in the vascular smooth muscle cells, hence, inducing cell apoptosis [6]. From the phytochemical viewpoint, curcumin is regarded as a safe active agent, because it has no toxic, genotoxic, or teratogenic properties. This suggests that curcumin could be used as a suitable model in various drug developments. However, the therapeutic potential of curcumin is

* Corresponding author.

E-mail address: mariayuliana@ukwms.ac.id (M. Yuliana).

^g These authors contributed equally to this work.

limited by its poor water solubility [7], poor oral bioavailability, and rapid degradation, limiting its clinical application [8]. To improve these properties, nanoparticle encapsulation and drug absorption to porous materials are generally employed to allow the effective delivery of curcumin. Flora et al. reported that the development of nano-encapsulation of curcumin for preclinical studies in cancer, inflammation, wound healing, and other diseases show an increased therapeutic efficacy when compared to non-encapsulated components [9]. Meanwhile, the drug absorption into a nano-sized porous carrier may improve the bioavailability of the drug, actively deliver the drugs to the target and work effectively at the target site, significantly enhancing the drug efficacy. Several porous carriers that have been studied include polymers [10], hydrogels [11], silica [12–14], and metal–organic frameworks (MOF) [15]. Several composite materials as the drug carrier have also been published, e.g. silica/chitosan nanocomposite [16], γ -cyclodextrin-based MOF/polyacrylic acid [17], and cellulose/MOF [18–20]. The latest offers several advantages compared to the other available composite nanocarriers, as it possesses (1) higher biocompatibility [21], (2) higher drug loading [22], and (3) lower cost compared to the synthetic nanomaterials [23,24] as cellulose, one of the constructing components in the composite, can be isolated from inexpensive natural resources [25–31], including coconut husk.

Indonesia generates more than 7 million tons of coconut husks annually, as reported by Zafar (2015) [32]. While being classified as one of the major wastes in the country, Pereira et al. reported that coconut husk has a composition of 36.78% cellulose, 33.11% hemicellulose, 31.34% lignin, 3.38% hot water soluble, and 0.15% ash [33], indicating the rich content of cellulose in this biomass, which can be converted further to various derivatives; one of them is cellulose microfibrils (CMF). CMF shows remarkable mechanical properties compared with other natural, glass, and carbon fibers [34]. Huang and Netravali (2009) reported the enhancement of the fracture stress resistance and the modulus of the soy protein concrete after the incorporation of bamboo-based CMF [35]. Meanwhile, Silviya et al. mentioned that the addition of CMF to the poly-(ethylene-co-vinyl acetate) increases the mechanical and thermal properties of the polymer [36]. Due to these superior characteristics, CMF finds extensive uses in various applications, including drug delivery. However, this material typically exhibits a burst drug release behavior in the initial stage, which is undesirable as it makes the total release time much shorter and reduces the bioavailability of the drug inside the system. Therefore, CMF is generally used in composite with other robust materials, including MOF, in drug delivery applications. Wu et al. mentioned that introducing MOF to the cellulose can enhance the dispersion and adhesion of the composite material, which may extend their functions [37].

MOF has shown great potential in various applications, including gas separation and storage, catalysis, chemical sensing, and adsorption [38]. It is also very suitable for use as a drug carrier, owing to its high chemical and thermal stability, large surface area, and tunable pore size [39–42]. This material is generally constructed by the coordination bonds between metal ions and organic ligands to form a one-, two-dimensional, or three-dimensional complex structure [43]. Various metal centers (alkaline earth metals, transition metals, and lanthanides) and organic ligands (carboxylates, phosphonates, and polyamines) can be used to create MOFs via different synthesis routes, which result in unique structural diversity [44,45]. Of several available MOF structures, zeolitic imidazolate framework-8 (ZIF-8) is selected in this research due to its sensitivity to pH [46], superior biocompatibility, and degradability [18], making it suitable for stimuli-targeted drug delivery. ZIF-8 is also known for its excellent performance in curcumin delivery; Tiwari et al., Duan et al., and Meng et al. have

reported the curcumin encapsulation into ZIF-8 structure and studied their potential as the anticancer and antibacterial agents [47–49]. However, despite its superiorities, ZIF-8 commonly exists in nanoparticle state and is difficult to separate [38]; the dispersing properties of ZIF-8 are also insufficient to control drug release. Therefore, a biocompatible matrix, e.g. CMF, is required for the ZIF-8 deposition to prevent the aggregation of ZIF-8 and, at the same time, improves its drug release ability. A study by Sultan et al. has shown the possibility of fabricating curcumin-loaded ZIF-8 scaffold via 3D printing with the support of nanocellulose, in which the results indicate its great potential in biomedical application [50]. On that account, we investigate the possibility of combining ZIF-8 and CMF, into a composite material, CMF/ZIF-8. Furthermore, few studies also suggest that functionalizing the surface of the material using (3-aminopropyl)-triethoxysilane (APTES) could increase drug loading capacity without changing structure [51]. Therefore, this present research will focus on the synthesis of APTES-functionalized CMF/ZIF-8 (hereinafter referred to as APTES-CMF/ZIF-8) and its potential in the curcumin uptake and release. The loading behavior of curcumin into APTES-CMF/ZIF-8 is evaluated at various temperatures (T , K), and the loading of APTES-CMF/ZIF-8 (m_c , % (w/w)), and illustrated via the kinetic, isotherm, and thermodynamic studies. Meanwhile, the release profile of curcumin is studied at two pH values, pH = 5.5 and pH = 7.4, to prove its responsiveness to pH.

2. Materials and methods

2.1. Materials

Coconut husk is purchased from a local coconut farm in Blitar, Indonesia. Sodium hydroxide (NaOH; 99 wt%), sulfuric acid (H_2SO_4 ; 96 wt%), hydrogen peroxide (H_2O_2 ; 50 wt%), sodium hypochlorite (NaClO; 12%), zinc nitrate hexahydrate ($Zn(NO_3)_2 \cdot 6H_2O$; 98%), 2-methylimidazole (99%), 2,2,6,6-tetramethylpiperidinyloxy (TEMPO; 99%), sodium bromide (NaBr; 99%), and APTES (99%) are obtained from Sigma-Aldrich (Germany). All chemicals are of analytical grades and used as received.

2.2. Preparation of CMF

Initially, the coconut husk is dried overnight at 110 °C and ground to obtain short fibers. The fibers are then dispersed in deionized water for 2 h at 50 °C to remove the impurities and subsequently filtered. The clean fibers are subjected to the microwave-assisted alkaline treatment (25 wt% NaOH solution, alkaline: fibers mass ratio of 30:1, 240 V, 800 W) for 1 h and decanted to separate the fibers from the supernatant. This procedure is repeated until the supernatant turns colorless; then, the delignified fibers are dried for 12 h at 110 °C.

Consecutively, 10 g of delignified fiber is bleached using the microwave-assisted method (240 V, 800 W) for 1 h, where the H_2O_2 solution (30 wt%, 300 mL) and two drops of 0.5 M NaOH solution are added at the beginning of the process. After the reaction time is reached, the resulting mixture is filtered to remove the supernatant. This cycle is employed until the white color is observed in the solid residue, and it is oven-dried for 12 h to obtain the cellulose fibers.

In a typical synthesis of CMF, 1.94 g of purified cellulose fibers and 100 mL of deionized water are mixed and sonicated for 5 min to promote the swelling of the cellulose. Meanwhile, 30 mg TEMPO and 100 mg NaBr are initially dissolved in 50 mL water and subsequently added to the cellulose/water mixture. To initiate the TEMPO oxidation, 14.2 mL of NaClO solution (12 wt%) is added to the mixture. The reaction is held for 30 min at pH = 10 (by adding

0.5 M HCl solution) and ambient temperature. The resulting suspension is then sonicated for 30 min, centrifuged (4900 rpm, 10 min), dialyzed against deionized water for 2 days, and oven-dried for 12 h to obtain CMF.

2.3. Synthesis of CMF/ZIF-8 and its direct functionalization by APTES

In a typical in-situ synthesis of CMF/ZIF-8, 0.5 g of cellulose is mixed with 3.94 g of 2-methylimidazole and 16 mL of deionized water for 15 min at room temperature. Meanwhile, the metal solution is prepared by dispersing 1.6 g of $Zn(NO_3)_2 \cdot 6H_2O$ in a mixture of 1.6 mL deionized water and 0.2 mL of 0.1 N NaOH solution. The above two suspensions are then combined and the total volume is adjusted into 50 mL using deionized water. This mixture is stirred for an hour at ambient temperature. The resulting solid product is collected by centrifugation at 4500 rpm for 10 min, repeatedly washed with ethanol, and oven-dried for 24 h at 85 °C to obtain the CMF/ZIF-8.

The functionalization of APTES onto the surface of CMF/ZIF-8 is achieved as follows. CMF/ZIF-8 (1.0 g) is dispersed in 100 mL ethanol under sonication for 30 min. The mixture is then heated to 95 °C until a quarter of the solution is evaporated, and the volume is adjusted back to 100 mL by adding ethanol. This cycle is repeated three times, after which 2 mL APTES is slowly added into the suspension. The mixture is continuously stirred for 24 h at 70 °C, before being washed twice with ethanol and dried in an oven at 60 °C to obtain the APTES-CMF/ZIF-8.

2.4. Characterization of APTES-CMF/ZIF-8

The morphology images of CMF and APTES-CMF/ZIF-8 are acquired using a JEOL JSM-6500F (Jeol Ltd., Japan) at an accelerating voltage of 10–20 kV and a working distance of 8.5–10.5 mm. The crystal structures of CMF, ZIF-8, and APTES-CMF/ZIF-8 are compared using the X-ray diffraction (XRD) analysis (X'PERT Analytical Pro X-ray diffractometer, Philips-FEI, Netherlands) at $2\theta = 5\text{--}60^\circ$, tube current = 30 mA, running voltage = 40 kV, and constant $Cu K_{\alpha 1}$ radiation, $\lambda = 1.5406 \text{ \AA}$. To measure the textural properties of APTES-CMF/ZIF-8, the N_2 sorption analysis is carried out at 77 K using a Micromeritics ASAP 2010 sorption analyzer (Micromeritics Instrument Corporation, USA) after degassing the sample for 2 h at 423 K.

2.5. Curcumin uptake study

The uptake behavior of curcumin onto APTES-CMF/ZIF-8 is characterized via kinetic and isotherm studies. All experimental batches are conducted using a 5-mL curcumin solution (1000 mg/L). The kinetic study is performed by adding $m_c = 0.1\%$ (w/w) of APTES-CMF/ZIF-8 to a series of curcumin solutions, with each batch collected at different time intervals ($t = 10\text{--}1440$ min). Meanwhile, the isotherm study uses various loading of APTES-CMF/ZIF-8 ($m_c = 0.1\text{--}1.0\%$ (w/w)) with adsorption time ($t = 1440$ min). Both studies are employed at three levels of temperature ($T = 30, 40, 50$ °C) to investigate the influence of temperature on curcumin uptake.

The adsorption capacities of APTES-CMF/ZIF-8 at a specific time (q_t , mg/g) and equilibrium (q_e , mg/g) can be calculated using equations (1) and (2).

$$q_t = \frac{(C_i - C_t)V}{m_s} \quad (1)$$

$$q_e = \frac{(C_i - C_e)V}{m_s} \quad (2)$$

where, C_i (mg/L) is the initial concentration of curcumin in solution, C_t (mg/L) and C_e (mg/L) are the concentration of curcumin in solution at a specific duration and at equilibrium, respectively. Meanwhile, V (L) is the volume of curcumin solution in the uptake process, and m_s (g) corresponds to the loaded mass of APTES-CMF/ZIF-8. Several kinetic and isotherm models are then employed to fit the data and evaluate the uptake behavior and mechanism.

Furthermore, three thermodynamic parameters, including Gibbs free energy (ΔG°), enthalpy (ΔH°), and entropy (ΔS°), are determined using the following equations (3)–(5).

$$\Delta G = -RT \ln K_c \quad (3)$$

$$K_c = \frac{q_e}{C_e} \quad (4)$$

$$\Delta G^\circ = \Delta H^\circ - T\Delta S^\circ \quad (5)$$

where, R (J/mol/K) is the ideal gas constant, T (K) is temperature, K_c is the adsorption distribution constant, q_e (mg/g) is the uptake capacity at equilibrium, and C_e (mg/L) is the concentration of curcumin in solution at equilibrium.

2.6. Release study of curcumin

The curcumin release from curcumin-loaded APTES-CMF/ZIF-8 (Cur@APTES-CMF/ZIF-8) is performed by introducing 200 mg Cur@APTES-CMF/ZIF-8 into a 5 mL phosphate-buffered saline (PBS) solution in a dialysis membrane. The membrane containing the loaded Cur@APTES-CMF/ZIF-8 is then immersed in 500 mL PBS solution and slowly stirred at a constant temperature of 37 °C. The PBS solution (5 mL) is withdrawn at various release duration with the range of 10 min to 9 days and analyzed using Shimadzu ultraviolet–visible spectrophotometer 2600 (Shimadzu, Japan) at a wavelength (λ) of 429 nm. The solution taken during sampling is replaced with the fresh PBS solution to maintain the constant volume of the release system. The release study is performed at two pH values (5.5 and 7.4) to simulate the blood plasma condition and to evaluate the pH-responsiveness characteristics of APTES-CMF/ZIF-8.

3. Results and discussions

3.1. Characterization of APTES-CMF/ZIF-8

The scanning electron microscopy images of CMF and APTES-CMF/ZIF-8 are presented in Fig. 1. The rod-like CMF has a uniform width, ranging from 5 to 10 μm and length up to several tens of microns (Fig. 1a and b). Meanwhile, Fig. 1c shows a clear difference between CMF and its cellulosic composite with ZIF-8, particularly in their surface roughness. It is apparent from the figure that APTES-CMF/ZIF-8 possesses a rough surface morphology, implying the successful in-situ impregnation of ZIF-8 on the surface of CMF. The image magnification of APTES-CMF/ZIF-8 (Fig. 1c—insert) reveals that the attached ZIF-8 particles are of rhombic dodecahedron shape with a particle diameter of 300–400 nm, which is consistent with the previous study by Song et al. [52].

Fig. 2a shows the supporting XRD profiles of CMF and APTES-CMF/ZIF-8. Both spectra display the characteristic peaks of CMF at $2\theta = 21^\circ$ and 22° which correspond to a crystal plane of 120 and

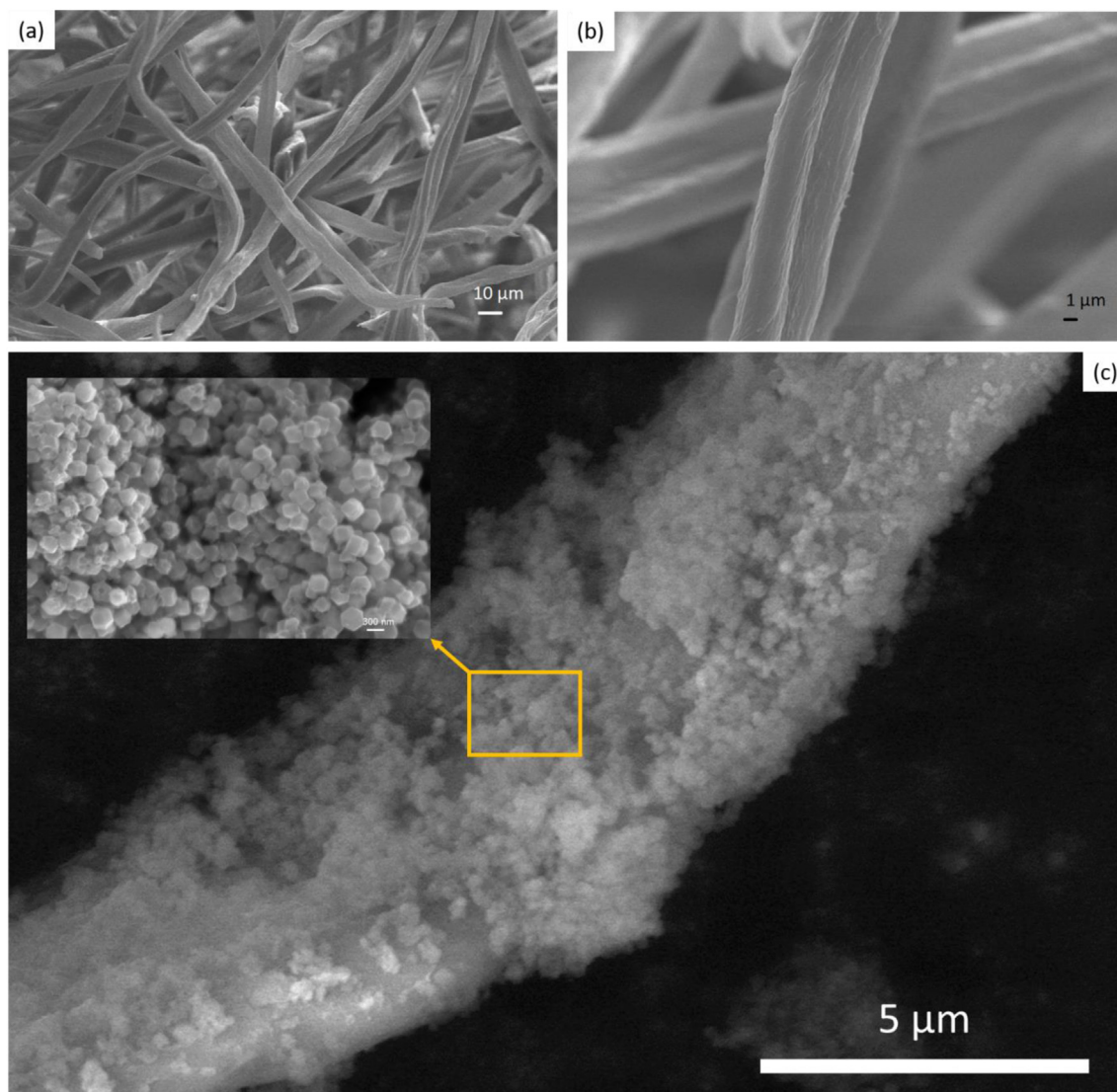


Fig. 1. SEM images of (a–b) coconut waste-based CMF at different magnifications, (c) APTES-CMF/ZIF-8 with the magnification on the morphological structure of ZIF-8 (inset). APTES-CMF/ZIF-8, coconut waste-based cellulose microfibrils and zeolitic imidazolate framework-8 functionalized with (3-aminopropyl)-triethoxysilane; SEM, scanning electron microscopy.

200 and are generally owned by the cellulosic materials. The two small peaks of CMF ($2\theta = 21^\circ, 22^\circ$) in the APTES-CMF/ZIF-8 diffraction profile imply that the ZIF-8 particles indeed have successfully covered the surface of CMF. This result is supported by the presence of strong peaks at $2\theta = 9^\circ$ (110), 11° (200), 14° (211), 15° (220), 16° ($1\bar{1}0$), and 17° (222) in the XRD analysis of composite material, indicating the existence of ZIF-8 on its surface.

The N_2 sorption measurement is performed to determine the porosity of APTES-CMF/ZIF-8. The surface area (S_{BET}) and pore volume (V_p) of APTES-CMF/ZIF-8 are obtained at $247.6 \text{ m}^2/\text{g}$ and $0.21 \text{ m}^3/\text{g}$, respectively. The N_2 adsorption/desorption profile (Fig. 2b) reveals a significant increase when p/p^0 is between 0–0.1 and 0.9–1.0, indicating that the test sample contains abundant mesopores [53]. This figure also implies that extensive multilayer adsorption is possible to happen inside the pores. The Barrett–Joyner–Halenda pore size distribution curve (Fig. 2c) confirms the availability of mesopore structures in the composite material, with an average pore width of 34.3 \AA (3.43 nm). However, an unusual phenomenon is observed in Fig. 2b, where desorption curve does not close at low p/p^0 . Jeromenok and Weber suggest

that the swelling of the polymer–polymer interaction within the cellulose matrix is the main cause of this opened hysteresis loop. The expansion of existing and/or the formation of new pores in the restricted-access (very narrow) openings will inversely cause the adsorbed component to be retained inside, as there is no thermodynamic reason for the adsorbate to be desorbed at low relative pressure, hence, causing the incomplete desorption [54]. Weber et al. also mention that the observed hysteresis is likely due to the formation of the hydrogen bonding within the polymer at higher pressure (during adsorption), which leads to the inability of the cellulose matrix to relax back into its original shape at low p/p^0 (during desorption) [55].

3.2. The uptake study of curcumin

The curcumin uptake is performed by stirring-assisted wet immersion of the APTES-CMF/ZIF-8 in curcumin solution. The camera images of the material before and after adsorption are presented in Fig. 3. The curcumin uptake data at various times are then fitted using several kinetic models (Fig. 4), e.g. pseudo-first-order (PFO),

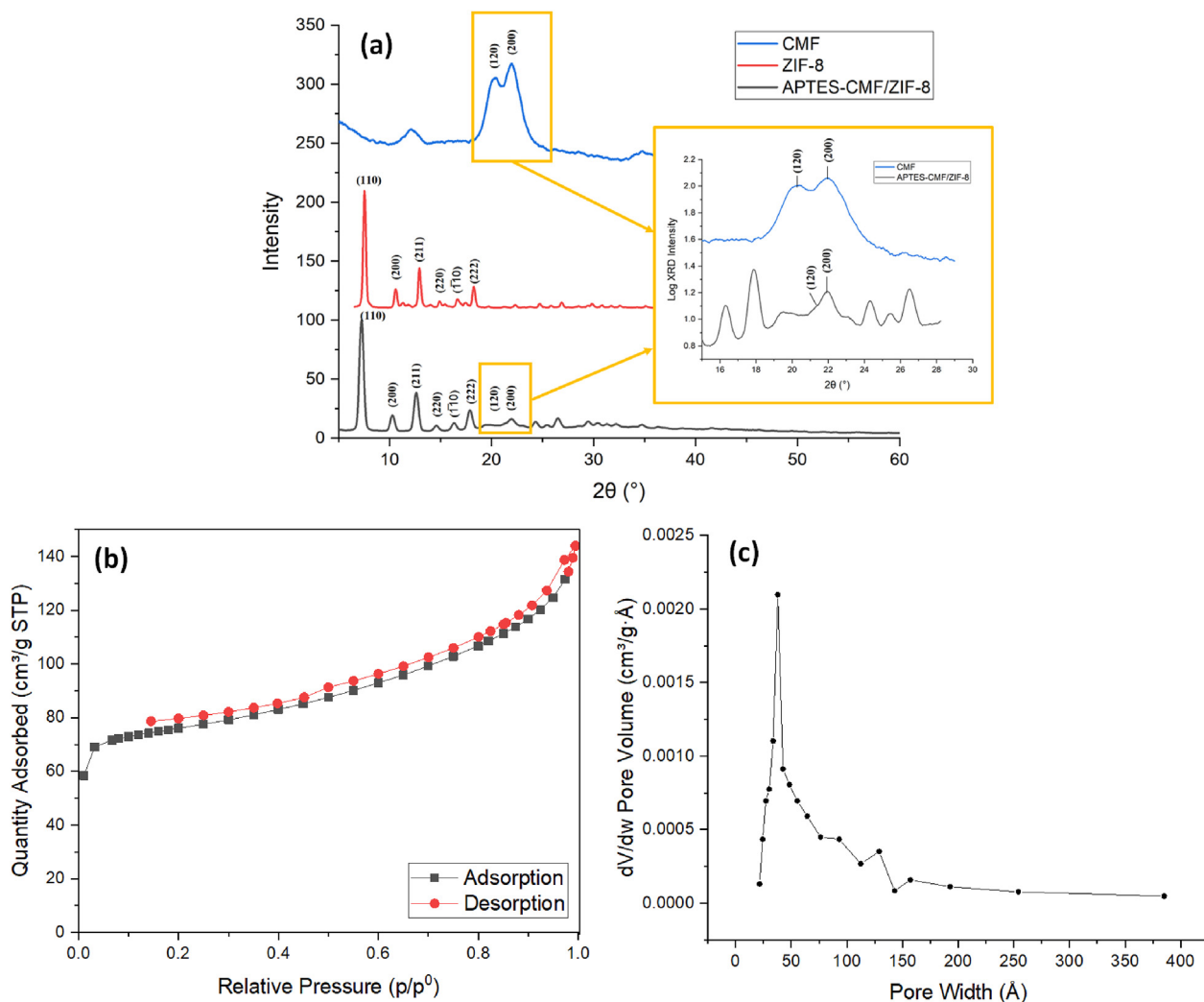


Fig. 2. (a) XRD spectra of CMF, ZIF-8, and APTES-CMF/ZIF-8, (b) N₂ adsorption/desorption profile, and (c) BJH pore size distribution curve of APTES-CMF/ZIF-8. APTES-CMF/ZIF-8, coconut waste-based cellulose microfibers and zeolitic imidazolate framework-8 functionalized with (3-aminopropyl)-triethoxysilane; BJH, Barret–Joyner–Halenda; XRD, X-ray diffraction.

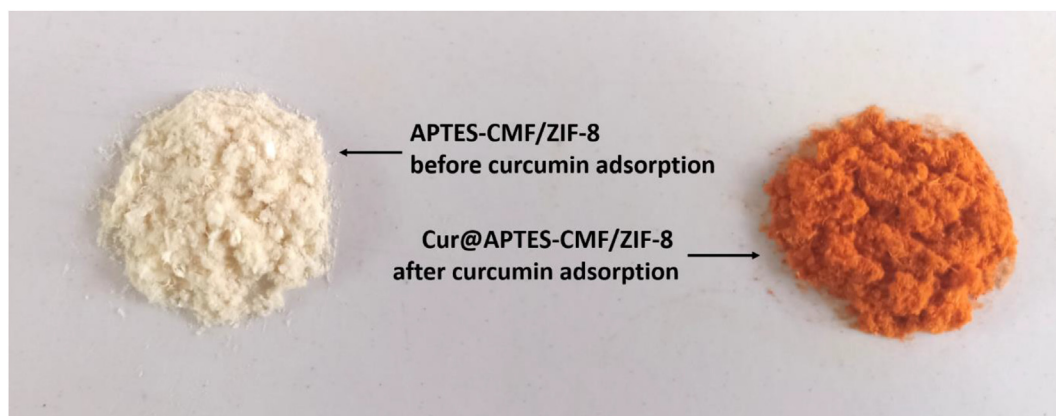


Fig. 3. The images of APTES-CMF/ZIF-8 before (left) and after (right) adsorption of curcumin. APTES-CMF/ZIF-8, coconut waste-based cellulose microfibers and zeolitic imidazolate framework-8 functionalized with (3-aminopropyl)-triethoxysilane.

pseudo-second-order (PSO), and intraparticle diffusion (IPD), with the tabulated parameters summarized in Table 1. As seen in Fig. 4, the uptake system shows an exponential increase in the adsorption

of curcumin during the first 240 min and reaches equilibrium condition after 1440 min regardless of the temperature. The loading capacity of curcumin is monitored to decrease by 1.5 folds

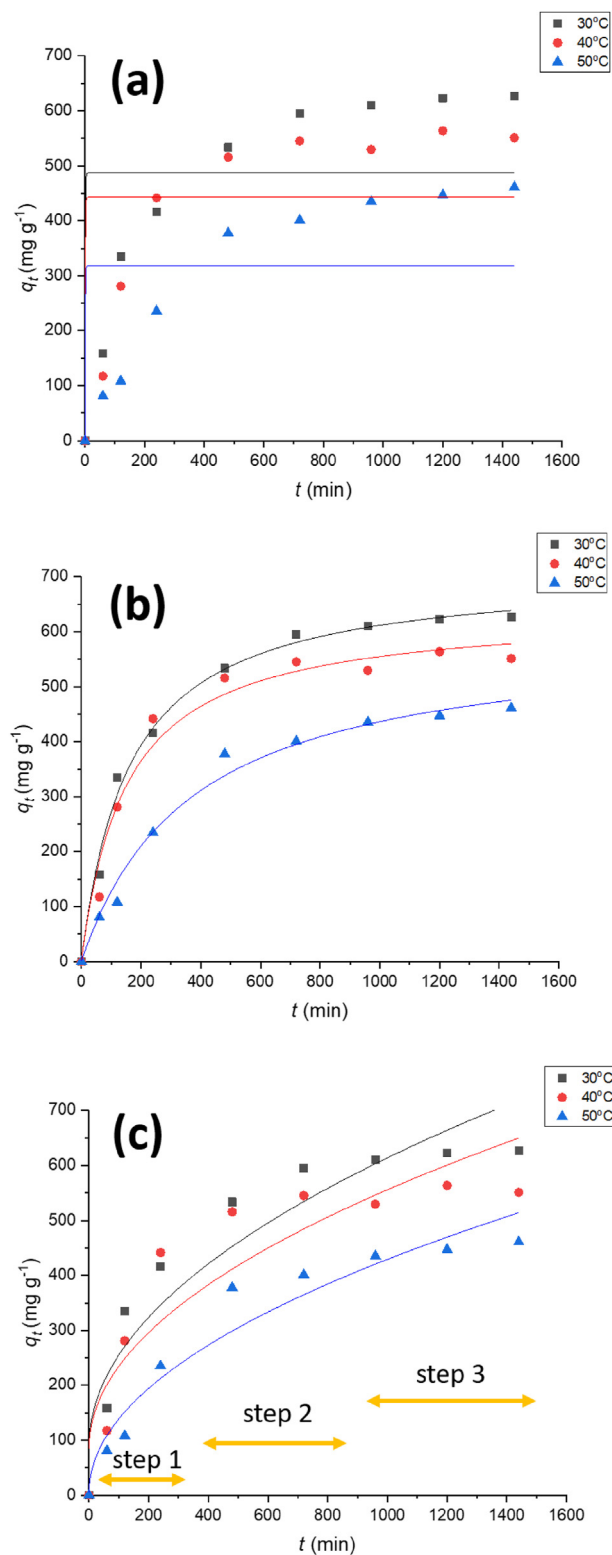


Fig. 4. The kinetic profile of the curcumin uptake onto APTES-CMF/ZIF-8, fitted to (a) PFO, (b) PSO, (c) IPD ($m_c = 0.1\%$ (w/w), initial curcumin concentration = 1000 mg/L). APTES-CMF/ZIF-8, coconut waste-based cellulose microfibers and zeolitic imidazolate framework-8 functionalized with (3-aminopropyl)-triethoxysilane; IPD, intraparticle diffusion; PFO, pseudo-first-order; PSO, pseudo-second-order.

when the temperature escalates from $T = 30$ to $T = 50$ °C, indicating a reduced diffusion rate of adsorbate across the external boundary layer of APTES-CMF/ZIF-8 at a higher temperature. This may also be

Table 1

The kinetic parameters of the curcumin uptake using APTES-CMF/ZIF-8 at various temperatures ($m_c = 0.1\%$ (w/w), initial curcumin concentration = 1000 mg/L).

Parameters	Temperature (K)		
	303	313	323
$q_{e,exp}$ (mg/g)	626.4	551.1	461.1
Pseudo-first-order			
q_e (mg/g)	487.3	443.2	318.3
k_1 (g/(mg min))	1	1	1
R^2	0.4395	0.4170	0.2552
Pseudo-second-order			
q_e (mg/g)	710.0	637.9	596.5
k_2 (g/(mg min))	1.04×10^{-5}	8.77×10^{-6}	4.57×10^{-6}
R^2	0.9926	0.9711	0.9849
Intraparticle diffusion (IPD)			
k_{IPD} (mg/(g min ^{1/2}))	13.43	14.86	16.60
- k_{IPD1}	27.93	28.57	14.32
- k_{IPD2}	1.05	1.05	1.11
- k_{IPD3}	2.37	3.20	3.66
C	89.20	85.97	4.69
R^2	0.8870	0.8168	0.9370

associated with the tendency of the curcumin to detach from the surface of APTES-CMF/ZIF-8 due to the excessive collision intensity between both adsorbate and adsorbent at higher temperatures [56,57]. Lee et al. also stated that the cellulose surface binding generally weakens along with the temperature enhancement [58].

Based on the R^2 value (Table 1), the experimental data show a better fit to the PSO model compared with the pseudo-first-order model, implying that the interaction between curcumin and APTES-CMF/ZIF-8 is of chemical nature, with the involvement of the electron transfer and/or exchange between curcumin and APTES-CMF/ZIF-8. The consistent trend of the computed data to the experimental results confirms the suitability of PSO in depicting the kinetic data of the curcumin uptake on APTES-CMF/ZIF-8. This model also suggests that the sorption capacity heavily depends on the number of active sites on the adsorbent. Further, the kinetic constants of PSO show a decrease along with the temperature, from $k_2 = 1.04 \times 10^{-5}$ g/(mg min) at $T = 30$ °C to $k_2 = 4.57 \times 10^{-6}$ g/(mg min) at $T = 50$ °C, which implies to the exothermic nature of the adsorption. The computed activation energy (E_a) is also obtained at 3.38 kJ/mol.

In this study, we use a multilinear IPD model to elaborate the adsorption steps, where the whole migration of curcumin from the bulk solution into the pores of APTES-CMF/ZIF-8 can be divided into three steps: (1) the fast transfer of curcumin from the bulk solution to the surface of APTES-CMF/ZIF-8, (2) the slow diffusion of curcumin from the boundary layer to the pores of APTES-CMF/ZIF-8, and (3) the chemical binding of curcumin molecules on the active sites of APTES-CMF/ZIF-8 via electron transfer. As seen in Table 1, the fitted adsorption constants of the three steps (k_{IPD1} , k_{IPD2} , and k_{IPD3} , respectively) show that k_{IPD1} is larger than the other two; a similar trend is monitored in all temperature levels. These results suggest that the diffusion of curcumin molecules from the bulk solution to the surface of APTES-CMF/ZIF-8 is the rate-governing step, followed consecutively by the chemical binding between curcumin and APTES-CMF/ZIF-8, and the slow intra-particle diffusion. The above-mentioned finding is supported by the Elovich theory, in which the rate of adsorption exponentially decreases with the increasing amount of curcumin adsorbed on the adsorbent surface [59]. Moreover, it can be observed that the IPD intercept constant (C) value escalates with the temperature rise. This constant linearly correlates with the influence of the boundary layer on the adsorption, where the higher the value, the greater the effect. Therefore, it can be concluded that by increasing the temperature, the boundary layer of APTES-CMF/ZIF-8 gives more barrier to the

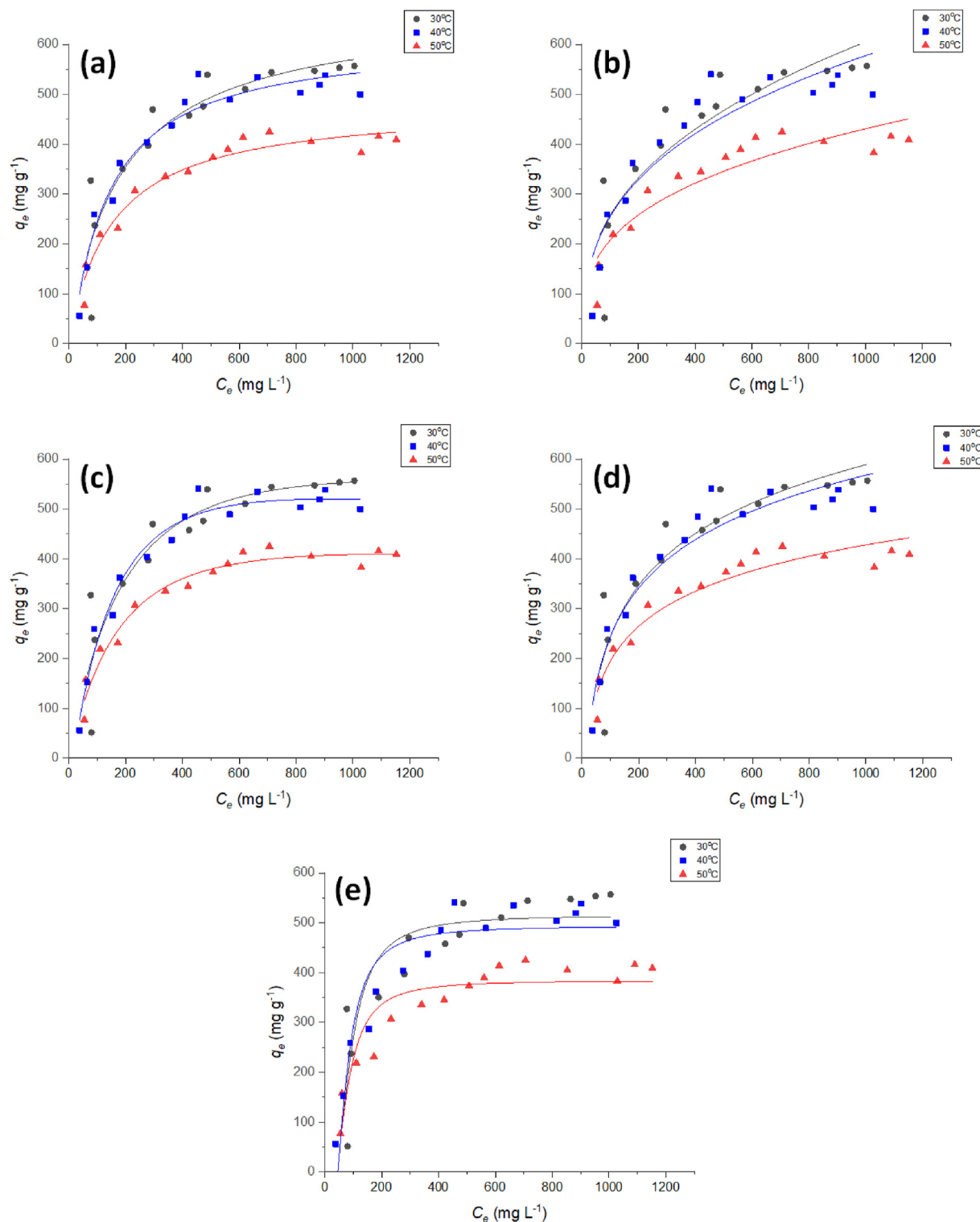


Fig. 5. The fitted isotherm models: (a) Langmuir, (b) Freundlich, (c) Redlich–Peterson, (d) Temkin, and (e) Dubinin–Radushkevich on the equilibrium data of curcumin uptake onto APTES-CMF/ZIF-8. APTES-CMF/ZIF-8, coconut waste-based cellulose microfibers and zeolitic imidazolate framework-8 functionalized with (3-aminopropyl)-triethoxysilane.

molecule diffusion, hence, lowering the amount of curcumin to be attached on the surface of APTES-CMF/ZIF-8. An exothermic nature of this uptake system can be monitored from the experimental data, as evidenced by the decreasing values of all kinetic constants (k_2 and k_{IPD}), and equilibrium adsorption capacity (q_e) along with the temperature from $T = 30\text{ }^\circ\text{C}$ to $T = 50\text{ }^\circ\text{C}$.

The isotherm profile of the curcumin uptake is presented in Fig. 5, while the calculated parameters are summarized in Table 2. Five fitting models, e.g. Langmuir, Freundlich, Redlich–Peterson (RP), Temkin, and Dubinin–Radushkevich (DR), are used to identify the adsorption behavior. According to Giles classification [60], the isotherm data represent the L-curve with subclass 2. This L-

Table 2

The computed isotherm parameters of curcumin uptake using APTES-CMF/ZIF-8 ($t = 1440$ min, initial concentration of curcumin = 1000 mg/g).

Isotherm	Parameters	Temperature (K)		
		303	313	323
Langmuir	$q_{m(L)}$ (mg/g)	672.6	536.9	479.9
	k_L (L/mg)	0.008	0.007	0.006
	r^2	0.8564	0.9554	0.9486
Freundlich	k_F ((mg/g) (L/mg) ^{1/n})	61.53	47.68	46.28
	$1/n_F$	0.305	0.319	0.372
	r^2	0.8438	0.8488	0.7936
Redlich-Peterson	k_{RP} (L/g)	3.28	3.05	2.43
	α_{RP} (L/mg) ^g	0.002	0.002	0.002
	g	1.18	1.17	1.15
	r^2	0.9656	0.8497	0.9547
	r^2	0.088	0.068	0.050
Temkin	k_T (L/g)	108.2	95.5	160.5
	E_T (J/mol)	108.2	95.5	160.5
	r^2	0.9212	0.9201	0.8439
Dubinin–Radushkevich	$q_{m(DR)}$ (mg/g)	515.6	440.8	384.4
	E_{DR} (kJ/mol)	0.444	0.531	0.499
	r^2	0.7973	0.8698	0.8462
	r^2	0.7973	0.8698	0.8462

curve demonstrates that the curcumin adsorption continuously increases along with its initial concentration (C_i) and the adsorption site availability until all binding sites reach their saturation capacity. Dabrowski et al. also mentioned that this isotherm profile elaborates the adsorption pathway of a solute toward the adsorbent surface, where in this case, the curcumin molecules are adsorbed aligned with the APTES-CMF/ZIF-8 surface and there is no competition between both adsorbate and solvent to attach on the binding sites of APTES-CMF/ZIF-8 [61]. Therefore, it can be concluded that the adsorption capacity of APTES-CMF/ZIF-8 towards curcumin mainly depends on the number of active sites present in the adsorbent, which is in agreement with the previous kinetic study.

Based on the R^2 value, the equilibrium data conform better to the Langmuir model than Freundlich, suggesting that curcumin uptake onto APTES-CMF/ZIF-8 follows a monolayer mechanism, and this sorption happens homogeneously within the surface of APTES-CMF/ZIF-8 [62]. Fig. 5a shows that the experimental and predicted q_e obtained using the Langmuir model share similar values, verifying the accuracy of this model to illustrate the curcumin uptake. The APTES-CMF/ZIF-8 surface homogeneity is also validated by the exponent constant of the RP model (g) whose values are close to unity at all temperatures. The decreasing values of maximum monolayer capacity ($q_{m(L)}$) and Langmuir constant (k_L) from 672.6 mg/g and 0.008 L/mg at $T = 30$ °C to 479.9 mg/g and 0.006 L/mg at $T = 50$ °C emphasize the exothermic nature of the uptake system. Similarly, all Freundlich (k_F), Temkin (k_T), and RP (k_{RP}) constants decline when the system is heated from $T = 30$ °C to $T = 50$ °C. The computed sorption intensity ($1/n_F$) is monitored at 0.305–0.372 within the tested temperatures, indicating that curcumin uptake is favorable [63].

The heat of sorption (E_T) and mean sorption energy (E_{DR}) are determined from the Temkin and DR regressions to confirm the nature of the curcumin uptake onto APTES-CMF/ZIF-8; the results are presented in Table 2. The E_T values are monitored between 108.2 and 160.5 J/mol at the temperature levels between 30 and 50 °C, lower than the minimum energy threshold of chemisorption (20 kJ/mol) mentioned by Atkins (1999) [64]. Meanwhile, all E_{DR} values within tested temperatures are found lower than 8 kJ/mol (0.444–0.531 kJ/mol), which also indicates the physical nature of the uptake [65]. These results indicate this uptake system is primarily driven by the physical interaction (the fast diffusion of curcumin from the bulk solution to the external boundaries of

Table 3

The thermodynamic parameters of the curcumin uptake onto APTES-CMF/ZIF-8.

Temperature (K)	Thermodynamic parameters		
	ΔG° (kJ/mol)	ΔH° (kJ/mol)	ΔS° (J/mol.K)
303	-20.227	-16.743	11.4
313	-20.298		
323	-20.456		

APTES-CMF/ZIF-8), rather than the chemical electron exchange between curcumin and APTES-CMF/ZIF-8.

The thermodynamic behavior of the uptake system is analyzed using the Gibbs free energy change (ΔG°), enthalpy (ΔH°), and entropy (ΔS°), and the results are given in Table 3. The negative values of ΔG° are observed at all temperatures, indicating that the migration of curcumin onto APTES-CMF/ZIF-8 happens spontaneously and favorably. A similar value of ΔG° as the temperature increases shows that the affinity of curcumin to APTES-CMF/ZIF-8 is stable within the tested temperature levels. Meanwhile, the negative value of ΔH° (-16.743 kJ/mol) confirms the exothermic nature of the system. The entropy (ΔS°) is also obtained at 11.4 J/mol.K, implying the decreased randomness of curcumin molecules on the surface of APTES-CMF/ZIF-8 at higher temperature levels.

3.3. Release study

The curcumin release from the curcumin-loaded APTES-CMF/ZIF-8 (Cur@APTES-CMF/ZIF-8) is carried out for 9 days at two pH values, 5.5 and 7.4, to elaborate the pH responsiveness of APTES-CMF/ZIF-8; the obtained release data are then plotted in Fig. 6. The drug release profile at both pHs exhibits a slow first-order release, where the curcumin is released at an accelerated rate in the early stage to quickly achieve the effective therapeutic concentration of curcumin, followed by the constant rate to maintain the curcumin concentration in the blood system and/or in target tissues at the desired value as long as possible [66–68]. This release pattern is beneficial because the drug can be released in a controlled manner. Such slow release may also reduce and even negate the probability of side-effects caused by an immediate burst release. Moreover, it can provide a stable therapeutic effect over a longer period.

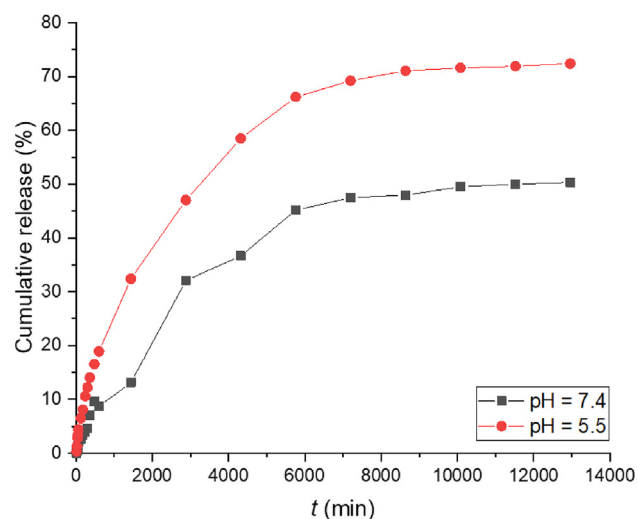


Fig. 6. The curcumin release profile from Cur@APTES-CMF/ZIF-8 at various pH. APTES-CMF/ZIF-8, coconut waste-based cellulose microfibers and zeolitic imidazolate framework-8 functionalized with (3-aminopropyl)-triethoxysilane.

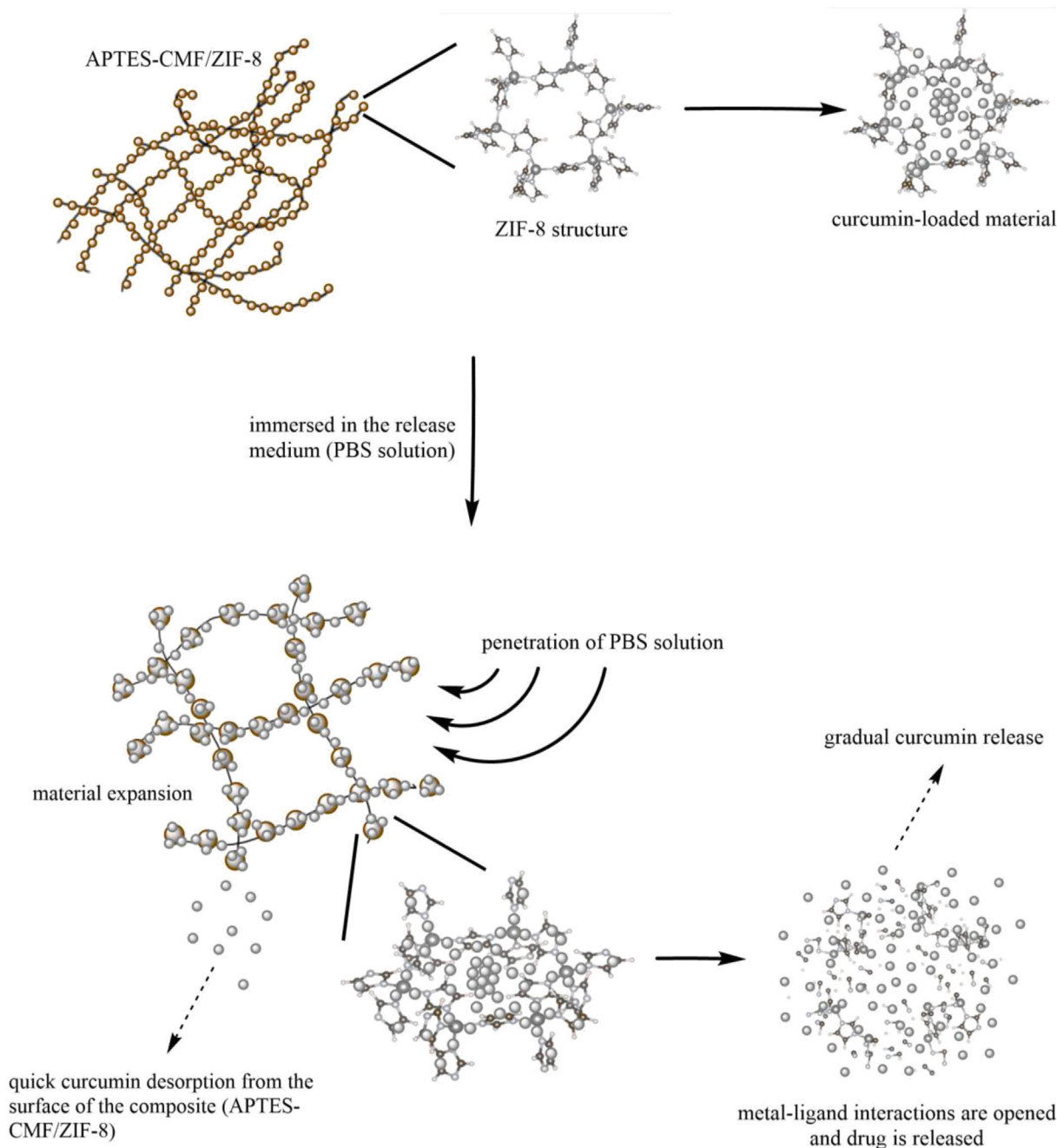


Fig. 7. The release mechanism of curcumin from Cur@APTES-CMF/ZIF-8 at pH 5.5. APTES-CMF/ZIF-8, coconut waste-based cellulose microfibers and zeolitic imidazolate framework-8 functionalized with (3-aminopropyl)-triethoxysilane.

Fig. 6 shows that the cumulative release reaches 74.2% at pH 5.5 and 47.9% at pH 7.4, signifying the pH-responsiveness behavior of APTES-CMF/ZIF-8. This stimuli responsiveness of the composite material provokes its metal–ligand coordination to open an acidic environment, which is beneficial for the delivery of the anticancer agent like curcumin as it prevents drug leakage/exposure to normal organs during delivery to the target. The curcumin release mechanism at pH 5.5 can be divided into five steps (Fig. 7) as follows: (1) the penetration of PBS solution into the pores of APTES-CMF/ZIF-8 which causes the composite material to swell and expand, (2) the interaction of curcumin molecules with the PBS solution, (3) the quick desorption of curcumin molecules from the surface of APTES-CMF/ZIF-8 into the medium in the initial phase of release, followed

consecutively by, (4) the opening of metal–ligand confinement in APTES-CMF/ZIF-8 due to its sensitivity to the acidic environment, and (5) the constant-rate dissolution of curcumin due to the gradual dissociation of APTES-CMF/ZIF-8 [69]. According to Butonova et al. and Velásquez-Hernández et al., following the dissociation is a possible slow decomposition of ZIF-8 to zinc phosphate sediment, which is a result from the bonding between the detached zinc ion from ZIF-8 and phosphate ion from PBS solution [70,71]. Butonova et al. added that the generated zinc phosphate exhibits mild cytotoxic effect to both tissue and cancer cells, and that lower amount of phosphate ions due to the sediment formation results in stronger suppression of the survival rate of both cells [70]. Despite its minimum downside to the tissue cells, this phenomenon may

assist the drug performance as an anticancer. Therefore, this study proves that the combination of pH-responsive ZIF-8 with the natural polymer matrix, CMF, can be used as promising materials for curcumin slow and controlled delivery.

4. Conclusions

APTES-CMF/ZIF-8 has been successfully fabricated using coconut husk waste as the cellulose source and sequentially employed for the uptake and release of curcumin. The coconut husk-derived cellulose has a uniform width (5–10 μm) and length (up to 10 μm). The synthesized APTES-CMF/ZIF-8 shares a similar fiber shape, but with a rougher surface due to the presence of rhombic dodecahedron-shaped ZIF-8 particles. The textural properties, e.g. surface area and pore volume, of CMF/ZIF-8 are obtained at 247.6 m^2/g and 0.21 m^3/g , respectively. Excellent performance of APTES-CMF/ZIF-8 as curcumin carrier is seen from the uptake capacity which reaches 626.4 mg/g at $m_c = 0.1\%$ (w/w), $t = 1440$ min, $T = 30$ °C, and initial curcumin concentration = 1000 mg/L . The curcumin loading to APTES-CMF/ZIF-8 obeys the PSO model and monolayer mechanism; their interaction is primarily governed by electron exchange/transfer. A slow and controlled release of curcumin using APTES-CMF/ZIF-8 is monitored in both pHs. The release study also shows that the cumulative release at pH 5.5 is significantly higher than that at pH 7.4, exhibiting the pH-responsive behavior of the composite. Therefore, APTES-CMF/ZIF-8 will be a potential smart drug carrier that can be implemented in a controlled drug delivery system with a stimuli-responsive mechanism. The valorization of coconut waste will also prominently reduce solid waste and turns a waste problem into a sustainable asset, in-country.

Credit author statement

Marvel Guntur Wijanarko. Conceptualization, methodology, software, visualization, investigation, writing – original draft.

Antonius Jimmy Widagdo. Conceptualization, methodology, software, visualization, investigation, writing – original draft.

Michael Suryananda Ismadji. Conceptualization, methodology, software, visualization, investigation, writing – original draft.

Karissa Kusuma. Methodology, software, visualization, investigation, writing – original draft.

Maria Yuliana. Conceptualization, methodology, software, visualization, writing-review and editing, resources, supervision.

Suryadi Ismadji. Project administration, funding acquisition.

Sandy Budi Hartono. Project administration, funding acquisition.

Jenni Lie. Software, investigation.

Hardy Shu. Software, investigation.

Hairus Abdullah. Software, investigation.

Grandprix Thomryes Marth Kadja. Software, investigation, validation.

Christian Julius Wijaya. Validation.

Felycia Edi Soetaredjo. Resources, data curation.

Declaration of competing interest

The authors declare that they have no known competing financial interests or personal relationships that could have appeared to influence the work reported in this paper.

Data availability

Data will be made available on request.

Acknowledgment

The authors thank the National Taiwan University of Science and Technology and Institut Teknologi Bandung for providing the facilities for material characterizations. This project was supported by the Ministry of Education, Culture, Research, and Technology of the Republic of Indonesia through research grant no. 260A/WM01.5/N/2022.

References

- [1] S. Prasad, S.C. Gupta, A.K. Tyagi, B.B. Aggarwal, Curcumin, a component of golden spice: from bedside to bench and back, *Biotechnol. Adv.* 32 (2014) 1053–1064, <https://doi.org/10.1016/j.biotechadv.2014.04.004>.
- [2] P. Anand, A.B. Kunnumakkara, R.A. Newman, B.B. Aggarwal, Bioavailability of curcumin: problems and promises, *Mol. Pharm.* 4 (2007) 807–818, <https://doi.org/10.1021/mp700113r>.
- [3] A. Kunwar, K.I. Priyadarsini, Curcumin and its role in chronic diseases, in: *Adv Exp Med Biol*, Springer New York LLC, 2016, pp. 1–25, https://doi.org/10.1007/978-3-319-41334-1_1.
- [4] M. Pulido-Moran, J. Moreno-Fernandez, C. Ramirez-Tortosa, M.C. Ramirez-Tortosa, Curcumin and health, *Molecules* 21 (2016), <https://doi.org/10.3390/molecules21030264>.
- [5] A.L. Lopresti, The problem of curcumin and its bioavailability: could its gastrointestinal influence contribute to its overall health-enhancing effects? *Adv. Nutr.* 9 (2018) 41–50, <https://doi.org/10.1093/advances/nmx011>.
- [6] D.K. Agrawal, P.K. Mishra, Curcumin and its analogues: potential anticancer agents, *Med. Res. Rev.* 30 (2010) 818–860, <https://doi.org/10.1002/med.20188>.
- [7] D. Akbik, M. Ghadiri, W. Chrzanowski, R. Rohanzadeh, Curcumin as a wound healing agent, *Life Sci.* 116 (2014) 1–7, <https://doi.org/10.1016/j.lfs.2014.08.016>.
- [8] Bhawana, R.K. Basniwal, H.S. Buttar, V.K. Jain, N. Jain, Curcumin nanoparticles: preparation, characterization, and antimicrobial study, *J. Agric. Food Chem.* 59 (2011) 2056–2061, <https://doi.org/10.1021/jf104402t>.
- [9] G. Flora, D. Gupta, A. Tiwari, Nanocurcumin: a Promising Therapeutic Advancement Over Native Curcumin, 2013. www.begellhouse.com.
- [10] N.D. Stebbins, M.A. Ouimet, K.E. Uhrich, Antibiotic-containing polymers for localized, sustained drug delivery, *Adv. Drug Deliv. Rev.* 78 (2014) 77–87, <https://doi.org/10.1016/j.addr.2014.04.006>.
- [11] V.L. Romero, R.H. Manzo, F.L. Allovero, Enhanced bacterial uptake and bactericidal properties of ofloxacin loaded on bioadhesive hydrogels against *Pseudomonas aeruginosa*, *J. Chemother.* 22 (2010) 328–334, <https://doi.org/10.1179/joc.2010.22.5.328>.
- [12] I.I. Slowing, B.G. Trewyn, S. Giri, V.S.Y. Lin, Mesoporous silica nanoparticles for drug delivery and biosensing applications, *Adv. Funct. Mater.* 17 (2007) 1225–1236, <https://doi.org/10.1002/adfm.200601191>.
- [13] N.I. Vazquez, Z. Gonzalez, B. Ferrari, Y. Castro, Synthesis of mesoporous silica nanoparticles by sol–gel as nanocontainer for future drug delivery applications, *Bol. Soc. Esp. Ceram. Vidr.* 56 (2017) 139–145, <https://doi.org/10.1016/j.bsecv.2017.03.002>.
- [14] M. Vallet-Regí, F. Balas, D. Arcos, Mesoporous materials for drug delivery, *Angew. Chem. Int. Ed.* 46 (2007) 7548–7558, <https://doi.org/10.1002/anie.200604488>.
- [15] A. Yildiz-Peköz, C. Ehrhardt, Advances in pulmonary drug delivery, *Pharmaceutics* 12 (2020) 1–7, <https://doi.org/10.3390/pharmaceutics12100911>.
- [16] S.A. Gaware, K.A. Rokade, S.N. Kale, Silica-chitosan nanocomposite mediated pH-sensitive drug delivery, *J. Drug Deliv. Sci. Technol.* 49 (2019) 345–351, <https://doi.org/10.1016/j.jddst.2018.11.022>.
- [17] H. Li, N. Lv, X. Li, B. Liu, J. Feng, X. Ren, T. Guo, D. Chen, J. Fraser Stoddart, R. Gref, J. Zhang, Composite CD-MOF nanocrystals-containing microspheres for sustained drug delivery, *Nanoscale* 9 (2017) 7454–7463, <https://doi.org/10.1039/c6nr07593b>.
- [18] Z. Karimzadeh, S. Javanbakht, H. Namazi, Carboxymethylcellulose/MOF-5/graphene oxide bio-nanocomposite as antibacterial drug nanocarrier agent, *BioImpacts* 9 (2019) 5–13, <https://doi.org/10.15171/bi.2019.02>.
- [19] S.A. Noorian, N. Hemmatinejad, J.A.R. Navarro, BioMOF@cellulose fabric composites for bioactive molecule delivery, *J. Inorg. Biochem.* 201 (2019), <https://doi.org/10.1016/j.jinorgbio.2019.110818>.
- [20] H.N. Abdelhamid, A.P. Mathew, Cellulose–metal organic frameworks (Cello-MOFs) hybrid materials and their multifaceted applications: a review, *Coord. Chem. Rev.* 451 (2022), <https://doi.org/10.1016/j.ccr.2021.214263>.
- [21] H.N. Abdelhamid, H.M. El-Bery, A.A. Metwally, M. Elshazly, R.M. Hathout, Synthesis of CdS-modified chitosan quantum dots for the drug delivery of sesamol, *Carbohydr. Polym.* 214 (2019) 90–99, <https://doi.org/10.1016/j.carbpol.2019.03.024>.
- [22] H.N. Abdelhamid, K.H. Hussein, Graphene oxide as a carrier for drug delivery of methotrexate, *Biointerface Res. Appl. Chem.* 11 (2021) 14726–14735, <https://doi.org/10.33263/BRIAC116.1472614735>.
- [23] H.N. Abdelhamid, Zeolitic imidazolate frameworks (ZIF-8, ZIF-67, and ZIF-L) for hydrogen production, *Appl. Organomet. Chem.* 35 (2021), <https://doi.org/10.1002/aoc.6319>.

- [24] D. Thassu, Y. Pathak, M. Deleers, Nanoparticulate Drug-Delivery Systems: an Overview, 2007.
- [25] N. Raghav, M.R. Sharma, J.F. Kennedy, Nanocellulose: a mini-review on types and use in drug delivery systems, *Carbohydr. Polym. Technol. Appl.* 2 (2021), 100031, <https://doi.org/10.1016/j.carpta.2020.100031>.
- [26] A.A. Sundarraj, T.V. Ranganathan, A review on cellulose and its utilization from agro-industrial waste, *Drug Invent. Today* 10 (2018) 89–94.
- [27] M.F. Rosa, E.S. Medeiros, J.A. Malmonge, K.S. Gregorski, D.F. Wood, L.H.C. Mattoso, G. Glenn, W.J. Orts, S.H. Imam, Cellulose nanowhiskers from coconut husk fibers: effect of preparation conditions on their thermal and morphological behavior, *Carbohydr. Polym.* 81 (2010) 83–92.
- [28] R. Liu, H. Yu, Y. Huang, Structure and morphology of cellulose in wheat straw, *Cellulose* 12 (2005) 25–34, <https://doi.org/10.1007/s10570-004-0955-8>.
- [29] M.S. Jahan, A. Saeed, Z. He, Y. Ni, Jute as raw material for the preparation of microcrystalline cellulose, *Cellulose* 18 (2011) 451–459, <https://doi.org/10.1007/s10570-010-9481-z>.
- [30] N.A. Bhimte, P.T. Tayade, Evaluation of microcrystalline cellulose prepared from sisal fibers as a tablet excipient: a technical note, *AAPS PharmSciTech* 8 (2007) 1–7, <https://doi.org/10.1208/pt0801008>.
- [31] J. Zhang, H. Song, L. Lin, J. Zhuang, C. Pang, S. Liu, Microfibrillated cellulose from bamboo pulp and its properties, *Biomass Bioenergy* 39 (2012) 78–83, <https://doi.org/10.1016/j.biombioe.2010.06.013>.
- [32] S. Zafar, Coconut Husk|BioEnergy Consult, 2015. <http://www.bioenergyconsult.com/tag/coconut-husk/>.
- [33] T.G.T. Pereira, D.W. Silva, T.M.C. Eugênio, M.V. Scatolino, I.C. de Carvalho Terra, C.S. Fonseca, L. Bufalino, R.F. Mendes, L.M. Mendes, Coconut fibers and quartzite wastes for fiber-cement production by extrusion, *Mater. Today Proc.* 31 (2019) S309–S314, <https://doi.org/10.1016/j.matpr.2020.01.394>.
- [34] N. Chand, M. Fahim, Green tribology and tribological characterization of biocomposites, in: N. Chand, M. Fahim (Eds.), *Tribology of Natural Fiber Polymer Composites*, second ed., Elsevier, 2021, pp. 207–212, <https://doi.org/10.1016/B978-0-12-818983-2.00009-8>.
- [35] X. Huang, A. Netravali, Biodegradable green composites made using bamboo micro/nano-fibrils and chemically modified soy protein resin, *Compos. Sci. Technol.* 69 (2009) 1009–1015, <https://doi.org/10.1016/j.compscitech.2009.01.014>.
- [36] E.K. Silviya, G. Unnikrishnan, S. Varghese, J.T. Guthrie, Thermal and mechanical characterization of EVA/banana fiber-derived cellulose composites, *J. Appl. Polym. Sci.* 125 (2012) 786–792, <https://doi.org/10.1002/app.35140>.
- [37] Y. Wu, Y. Li, T. Zhao, X. Wang, V.I. Isaeva, L.M. Kustov, J. Yao, J. Gao, Bimetal-organic framework-derived nanotube@cellulose aerogels for peroxymonosulfate (PMS) activation, *Carbohydr. Polym.* 296 (2022), <https://doi.org/10.1016/j.carbpol.2022.119969>.
- [38] W. Ren, J. Gao, C. Lei, Y. Xie, Y. Cai, Q. Ni, J. Yao, Recyclable metal-organic framework/cellulose aerogels for activating peroxymonosulfate to degrade organic pollutants, *Chem. Eng. J.* 349 (2018) 766–774, <https://doi.org/10.1016/j.cej.2018.05.143>.
- [39] L. Wang, M. Zheng, Z. Xie, Nanoscale metal-organic frameworks for drug delivery: a conventional platform with new promise, *J. Mater. Chem. B* 6 (2018) 707–717, <https://doi.org/10.1039/c7tb02970e>.
- [40] W. Cai, J. Wang, C. Chu, W. Chen, C. Wu, G. Liu, Metal-organic framework-based stimuli-responsive systems for drug delivery, *Adv. Sci.* 6 (2019), <https://doi.org/10.1002/advs.201801526>.
- [41] R.C. Huxford, J. Della Rocca, W. Lin, Metal-organic frameworks as potential drug carriers, *Curr. Opin. Chem. Biol.* 14 (2010) 262–268, <https://doi.org/10.1016/j.cbpa.2009.12.012>.
- [42] S. Mallakpour, E. Nikkhoo, C.M. Hussain, Application of MOF materials as drug delivery systems for cancer therapy and dermal treatment, *Coord. Chem. Rev.* 451 (2022), 214262, <https://doi.org/10.1016/j.ccr.2021.214262>.
- [43] H. Furukawa, K.E. Cordova, M. O’Keeffe, O.M. Yaghi, The chemistry and applications of metal-organic frameworks, *Science* 341 (2013), <https://doi.org/10.1126/science.1230444>.
- [44] M.B. Ram, K. Gupta, Tahir Rasheed, Tuan Anh Nguyen, Metal-Organic Frameworks-Based Hybrid Materials for Environmental Sensing and Monitoring, 2006.
- [45] E. Gulcay, I. Erucar, Metal-organic Frameworks for Biomedical Applications, Elsevier B.V., 2019, <https://doi.org/10.1016/B978-0-12-817650-4.00006-1>.
- [46] H. Kaur, G.C. Mohanta, V. Gupta, D. Kukkar, S. Tyagi, Synthesis and characterization of ZIF-8 nanoparticles for controlled release of 6-mercaptopurine drug, *J. Drug Deliv. Sci. Technol.* 41 (2017) 106–112, <https://doi.org/10.1016/j.jddst.2017.07.004>.
- [47] A. Tiwari, A. Singh, N. Garg, J.K. Randhawa, Curcumin encapsulated zeolitic imidazolate frameworks as stimuli responsive drug delivery system and their interaction with biomimetic environment, *Sci. Rep.* 7 (2017), <https://doi.org/10.1038/s41598-017-12786-6>.
- [48] S. Duan, S. Duan, X. Zhao, Z. Su, C. Wang, Y. Lin, Layer-by-layer decorated nanoscale ZIF-8 with high curcumin loading effectively inactivates gram-negative and gram-positive bacteria, *ACS Appl. Bio Mater.* 3 (2020) 3673–3680, <https://doi.org/10.1021/acsabm.0c00300>.
- [49] X. Meng, J. Guan, S. Lai, L. Fang, J. Su, pH-responsive curcumin-based nanoscale ZIF-8 combining chemophotodynamic therapy for excellent antibacterial activity, *RSC Adv.* 12 (2022) 10005–10013, <https://doi.org/10.1039/d1ra09450e>.
- [50] S. Sultan, H.N. Abdelhamid, X. Zou, A.P. Mathew, CelloMOF, Nanocellulose enabled 3D printing of metal-organic frameworks, *Adv. Funct. Mater.* 29 (2019), <https://doi.org/10.1002/adfm.201805372>.
- [51] Y. Wang, Y. Sun, J. Wang, Y. Yang, Y. Li, Y. Yuan, C. Liu, Charge-reversal APTES-modified mesoporous silica nanoparticles with high drug loading and release controllability, *ACS Appl. Mater. Interfaces* 8 (2016) 17166–17175, <https://doi.org/10.1021/acsami.6b05370>.
- [52] Y. Song, J.Y. Seo, H. Kim, K.Y. Beak, Structural control of cellulose nanofibrous composite membrane with metal organic framework (ZIF-8) for highly selective removal of cationic dye, *Carbohydr. Polym.* 222 (2019), <https://doi.org/10.1016/j.carbpol.2019.115018>.
- [53] R. Khatun, P. Bhanja, P. Mondal, A. Bhaumik, D. Das, S. Manirul Islam, Palladium nanoparticles embedded over mesoporous TiO₂ for chemical fixation of CO₂ under atmospheric pressure and solvent-free conditions, *New J. Chem.* 41 (2017) 12937–12946, <https://doi.org/10.1039/C7NJ02459B>.
- [54] J. Jeromenok, J. Weber, Restricted access: on the nature of adsorption/desorption hysteresis in amorphous, microporous polymeric materials, *Langmuir* 29 (2013) 12982–12989, <https://doi.org/10.1021/la402630s>.
- [55] J. Weber, N. Du, M.D. Guiver, Influence of intermolecular interactions on the observable porosity in intrinsically microporous polymers, *Macromolecules* 44 (2011) 1763–1767, <https://doi.org/10.1021/ma101447h>.
- [56] U.A. Edet, A.O. Ifeibuegu, Kinetics, isotherms, and thermodynamic modeling of the adsorption of phosphates from model wastewater using recycled brick waste, *Processes* 8 (2020) 665, <https://doi.org/10.3390/pr8060665>.
- [57] S. Karaca, A. Gürses, M. Ejder, M. Açıkyıldız, Kinetic modeling of liquid-phase adsorption of phosphate on dolomite, *J. Colloid Interface Sci.* 277 (2004) 257–263, <https://doi.org/10.1016/j.jcis.2004.04.042>.
- [58] H.J. Lee, H.S. Lee, J. Seo, Y.H. Kang, W. Kim, T.H.K. Kang, State-of-the-art of cellulose nanocrystals and optimal method for their dispersion for construction-related applications, *Appl. Sci.* 9 (2019) 1–14, <https://doi.org/10.3390/app9030426>.
- [59] F.C. Wu, R.L. Tseng, R.S. Juang, Characteristics of Elovich equation used for the analysis of adsorption kinetics in dye-chitosan systems, *Chem. Eng. J.* 150 (2009) 366–373, <https://doi.org/10.1016/j.cej.2009.01.014>.
- [60] B.C. H Giles, T.H. Macewan, S.N. Nakhwa, D. Smith, Solution adsorption isotherms, and its use in diagnosis of adsorption mechanisms and in measurement of specific surface areas of solids, *J. Chem. Soc.* (1960) 3973–3993.
- [61] A. Dabrowski, P. Podkościelny, Z. Hubicki, M. Barczak, Adsorption of phenolic compounds by activated carbon – a critical review, *Chemosphere* 58 (2005) 1049–1070, <https://doi.org/10.1016/j.chemosphere.2004.09.067>.
- [62] R. Rusmin, B. Sarkar, Y. Liu, S. McClure, R. Naidu, Structural evolution of chitosan-palygorskite composites and removal of aqueous lead by composite beads, *Appl. Surf. Sci.* 353 (2015) 363–375, <https://doi.org/10.1016/j.japsusc.2015.06.124>.
- [63] L. Widyayningsih, A. Setiawan, S.P. Santoso, F.E. Soetaredjo, S. Ismadij, S.B. Hartono, P.L. Tran-Nguyen, M. Yuliana, Feasibility study of nanocrystalline cellulose as adsorbent of steryl glucosides from palm-based biodiesel, *Renew. Energy* 154 (2020) 99–106.
- [64] P. Atkins, *Physical Chemistry*, sixth ed., Oxford University Press, London, 1999.
- [65] S. Chowdhury, R. Mishra, P. Saha, P. Kushwaha, Adsorption thermodynamics, kinetics and isosteric heat of adsorption of malachite green onto chemically modified rice husk, *Desalination* 265 (2011) 159–168, <https://doi.org/10.1016/j.desal.2010.07.047>.
- [66] S. Dash, P.N. Murthy, L. Nath, P. Chowdhury, Kinetic modeling on drug release from controlled drug delivery systems, *Acta Pol. Pharm. Drug Res.* 67 (2010) 217–223.
- [67] H. Maeda, M. Brandon, A. Sano, Design of controlled-release formulation for ivermectin using silicone, *Int. J. Pharm.* 261 (2003) 9–19, [https://doi.org/10.1016/S0378-5173\(03\)00293-X](https://doi.org/10.1016/S0378-5173(03)00293-X).
- [68] R. Langer, D. Wise, *Medical Applications of Controlled Release*, first ed., CRC Press, Boca Raton, 1984 <https://doi.org/10.1201/9780429276651>.
- [69] J. Zhuang, C.H. Kuo, L.Y. Chou, D.Y. Liu, E. Weerapana, C.K. Tsung, Optimized metal-organic-framework nanospheres for drug delivery: evaluation of small-molecule encapsulation, *ACS Nano* 8 (2014) 2812–2819, <https://doi.org/10.1021/nn406590q>.
- [70] S.A. Butonova, E.V. Ikonnikova, A. Sharsheeva, I.Y. Chernyshov, O.A. Kuchur, I.S. Mukhin, E. Hey-Hawkins, A.V. Vinogradov, M.I. Morozov, Degradation kinetic study of ZIF-8 microcrystals with and without the presence of lactic acid, *RSC Adv.* 11 (2021) 39169–39176, <https://doi.org/10.1039/d1ra07089d>.
- [71] M.D.J. Velásquez-Hernández, R. Ricco, F. Carraro, F.T. Limpoco, M. Linares-Moreau, E. Leitner, H. Wiltse, J. Rattenberger, H. Schröttner, P. Frühwirth, E.M. Stadler, G. Gescheidt, H. Amenitsch, C.J. Doonan, P. Falcaro, Degradation of ZIF-8 in phosphate buffered saline media, *CrystEngComm* 21 (2019) 4538–4544, <https://doi.org/10.1039/c9ce00757a>.